

Jet fragmentation and QCD models in e^+e^- annihilation at c.m. energies between 12.0 and 41.5 GeV

TASSO Collaboration

W. Braunschweig, R. Gerhards, F.J. Kirschfink, H.-U. Martyn

I. Physikalisches Institut der RWTH Aachen, 5100 Aachen, Federal Republic of Germany^a

B. Bock¹, H.M. Fischer, H. Hartmann, J. Hartmann, E. Hilger, A. Jocksch, R. Wedemeyer

Physikalisches Institut der Universität Bonn, 5300 Bonn, Federal Republic of Germany^a

B. Foster, A.J. Martin, A.J. Sephton

H.H. Wills Physics Laboratory, University of Bristol, Bristol BS8 1TL, UK^b

E. Bernardi, J. Chwastowski², A. Eskreys³, K. Gather, K. Genser⁴, H. Hultschig, P. Joos, H. Kowalski, A. Ladage, B. Löhr, D. Lüke, P. Mättig⁵, D. Notz, J.M. Pawlak⁶, K.-U. Pösnecker, E. Ros, D. Trines, R. Walczak⁴, G. Wolf

Deutsches Elektronen-Synchrotron, DESY, 2000 Hamburg, Federal Republic of Germany

H. Kolanoski

Institut für Physik, Universität Dortmund, Federal Republic of Germany^a

T. Kracht⁷, J. Krüger, E. Lohrmann, G. Poelz, W. Zeuner

II. Institut für Experimentalphysik der Universität Hamburg, 2000 Hamburg, Federal Republic of Germany^a

J. Hassard, J. Shulman, D. Su

Department of Physics, Imperial College, London SW7 2AZ, UK^b

F. Barreiro, A. Leites, J. del Peso

Universidad Autonoma de Madrid, Madrid, Spain^c

C. Balkwill, M.G. Bowler, P.N. Burrows, R.J. Cashmore, G.P. Heath, P.N. Ratoff, I.M. Silvester, I.R. Tomalin, M.E. Veitch

Department of Nuclear Physics, Oxford University, Oxford OX1 3RH, UK^b

G.E. Forden⁸, J.C. Hart, D.H. Saxon

Rutherford Appleton Laboratory, Chilton, Didcot, Oxon OX11 0QX, UK^b

S. Brandt, M. Holder, L. Labarga⁹

Fachbereich Physik der Universität-Gesamthochschule Siegen, 5900 Siegen, Federal Republic of Germany^a

Y. Eisenberg, U. Karshon, G. Mikenberg, A. Montag, D. Revel, E. Ronat, A. Shapira, N. Wainer, G. Yekutieli
Weizmann Institute, Rehovot 76100, Israel^d

D. Muller, S. Ritz, D. Strom¹⁰, M. Takashima, Sau Lan Wu, G. Zobernig

Department of Physics, University of Wisconsin, Madison, WI 53706, USA^e

Received 16 August 1988

¹ Now at Krupp Atlas Elektr. GmbH, Breen, FRG

² On leave from Inst. of Nuclear Physics, Cracow, Poland

³ Now at Inst. of Nuclear Physics, Cracow, Poland

⁴ Now at Warsaw University, Poland

⁵ Now at IPP Canada, Carleton University, Ottawa, Canada

⁶ On leave from Warsaw University^f, Poland

⁷ Now at Hasylab, DESY, Hamburg, FRG

⁸ Now at SUNY Stony Brook, Stony Brook, NY, USA

⁹ Now at SLAC, Stanford, CA, USA

¹⁰ Now at University of Chicago, Chicago, IL, USA

^a Supported by the Bundesministerium für Forschung und Technologie

^b Supported by the UK Science and Engineering Research Council

^c Supported by CAICYT

^d Supported by the Minerva Gesellschaft für Forschung mbH

^e Supported by the US Dept. of Energy, contract DE-AC02-76ER00881 and by the U.S. National Science Foundation Grant no. INT-8313994 for travel

^f Partially supported by grant CPBP 01.06

Abstract. The large amount of data accumulated by the TASSO detector at 35 GeV c.m. energy has been compared with the predictions of the latest generation of perturbative QCD + fragmentation models. By adjustment of the arbitrary parameters of these models, a very good description of the global properties of hadronic events was obtained. No one model gave the best description of all features of the data, each model being better than the others for some observables and worse in other quantities. We interpret these results in terms of the underlying QCD and hadronisation schemes. The trends of the data across the energy range $12.0 \leq W \leq 41.5$ GeV are generally well reproduced by the models with the parameters optimised at 35 GeV.

1 Introduction

In the last 10 years a wealth of information has been collected at PETRA and PEP on hadron production in high energy e^+e^- annihilation. The process $e^+e^- \rightarrow \gamma/Z \rightarrow \text{hadrons}$ is well described by models which incorporate perturbative QCD for the production of partons and a phenomenological hadronisation scheme for the transformation of the partons into the observed final state particles. Many studies of the properties of hadronic final states have been performed [1–5] and comparisons made with the QCD fragmentation models [6–8]. With the benefit of these analyses the authors are constantly updating and improving their models.

In this paper we compare distributions of physical quantities obtained from the 1986 TASSO hadronic data with the predictions of the most up to date QCD fragmentation models. A related study of multijet production is presented elsewhere [23]. The most important of the arbitrary parameters of these models were first optimised to provide a good description of a few relevant quantities, and then the models were tested more globally in terms of many observables. In Sect. 2 we briefly review the important features of the models, and define the observables in Sect. 3. Particle and event selection criteria are mentioned in Sect. 4, whilst backgrounds to the data sample, the parameter tuning and data correction procedures are described in Sects. 5, 6, 7 respectively. The results of the comparison between data and models at $W=35$ GeV are given in Sect. 8, whilst the energy evolution across the PETRA range is discussed in Sect. 9. We end with a summary and conclusions in Sect. 10. The model predictions for c.m. energies up to 200 GeV, using the parameters optimised at 35 GeV, are presented in [32].

2 QCD fragmentation models

The most widely used QCD fragmentation models are those of Webber [9], the Lund group [10] and Gottschalk [11]. A previous study [8] has shown that the Gottschalk model is unable to reproduce satisfactorily most features of hadronic events at $\sqrt{s}=29$ GeV and this model will not be considered further here. In this section we briefly mention important features of the Webber and Lund models; for a general review of fragmentation models see [12].

2.1 The Webber model

We consider version 4.2 of the program BIGWIG, implementing the physics in [9]. In the primary process $e^+e^- \rightarrow \gamma/Z \rightarrow q\bar{q}$ the initial quark and antiquark are assigned maximum allowed virtualities according to a particular distribution and are boosted to a frame in which their directions are perpendicular. One consequence of this is that the model does not preserve strict Lorentz invariance. It has been shown [7] that the final hadronic system is sensitive to the virtuality assignment and the boost factor γ , though we do not consider these issues here.

The off-mass-shell quarks then emit gluons, which may themselves radiate other gluons or split to $q\bar{q}$ pairs, producing a ‘parton cascade’ or ‘parton shower’ which evolves according to the Altarelli-Parisi equations [13] based upon the QCD Leading Logarithm Approximation (LLA). Parton virtualities thereby decrease by bremsstrahlung as the cascade evolves, the process being stopped when the virtuality of each parton falls below a cutoff value Q_0 , whence it is put on mass shell.

Soft gluon interference terms are included by the imposition of ‘angular ordering’ of the parton branchings, i.e. the angle θ_i between two daughter partons in a branching i is less than the angle at the previous branching, the very first branching angle being set at 90° by the boost. This requirement restricts the phase space for soft gluon emission, which corresponds physically to gluons of long wavelength being unable to resolve the individual colour charges of the partons in the cascade, which therefore acts coherently for soft gluon production. It has been shown that such a ‘coherent’ cascade model with cluster hadronisation is able to reproduce the ‘string effect’ [6], the depletion of particles in the region opposite the gluon-assigned jet in planar 3-jet events in e^+e^- , whilst a cascade + cluster model without the interference (a ‘conventional’ or ‘incoherent’ cascade) shows no such depletion. The interference effects are small at PETRA energies, even at the parton level

[14], and are diminished by hadronisation [15], though they may be large at very high energies [16].

α_s is allowed to ‘run’ throughout the cascade, the first-order formula:

$$\alpha_s(Q^2) = \frac{12\pi}{(33 - 2N_f) \ln\left(\frac{Q^2}{\Lambda_{LL}^2}\right)}$$

being used at each branching, with Q^2 decreasing at successive branchings. N_f is the number of active flavours and Λ_{LL} is the LLA QCD scale parameter, which is *not* equivalent to $\Lambda_{\overline{MS}}$ used in second order matrix element calculations. There is some degree of theoretical arbitrariness as to the choice of Q^2 scale; in this model $Q^2 \simeq p_T^2$ is used, as it is suggested [17] that this choice may effectively take into account higher order corrections to the interference effects.

At the termination of the cascade, when all partons have been put on mass shell, all gluons are split into $q\bar{q}$ pairs, each parton then joining with a neighbour of the correct colour index to form a colourless cluster. Heavy quarks (b, c) are then decayed. Clusters whose mass exceeds a certain value M_c are split into two and all clusters are allowed to decay by phase space, via resonances, to stable final state particles.

The three most important arbitrary parameters in the Webber model are hence the cascade virtuality cutoff Q_0 , the LLA scale parameter Λ_{LL} and the cluster mass parameter M_c . Alternative prescriptions for setting up the cascade within the basic framework of the Webber model involve other parameters [7, 18], but these will not be considered here.

(A new program incorporating a revised model with additional QCD features [30] has been made available only very recently, and hence we do not show any results in this paper.)

2.2 The Lund cascade model

The latest Lund cascade model [15] is included as a parton-level generator option in JETSET version 6.3 [10]. The cascade evolves according to the Altarelli-Parisi equations as for the Webber model, though here the similarity ends. There is no boosting of the initial $q\bar{q}$ pair to a frame in which they are at 90°. Instead the first parton branching is defined by matching the cascade onto the exact $O(\alpha_s)$ matrix element by using a rejection technique [15]. The angular ordering of successive branchings is similarly imposed by a rejection method. The evolution variable z is defined in terms of four-momentum products and the whole process is Lorentz invariant, though the gauge changes from one vertex to the next. The model has two arbitrary parameters: the virtuality

cutoff Q_0 and the LLA scale parameter Λ_{LL} , though there are certain theoretical degrees of freedom in the treatment of the kinematics of the cascade evolution, as well as in the choice of Q^2 scale for α_s . We have used the prescriptions chosen in the default version of JETSET [19], where e.g. $Q^2 \simeq p_T^2$.

At the termination of parton production, a colour triplet string is stretched between the final quarks, the gluons being kinks on the string, with the correct colour ordering. The string is then fragmented according to the Lund recipe [20] to obtain the final state hadrons. The parameters which were considered in the model optimisation procedure were a, b in the symmetric Lund fragmentation function:

$$f(x) = \frac{1}{x} (1-x)^a \exp\left(-\frac{bm_T^2}{x}\right)$$

used for *all* flavours, and σ , the width of the Gaussian p_T spectrum for primary quarks $\sim e^{-p_T^2/2\sigma^2} \cdot (m_T^2 = p_T^2 + m^2)$ is the hadron transverse mass-squared). The other string fragmentation parameters, such as the strange quark- and various diquark-suppression factors, are of secondary importance to the inclusive global properties of hadronic final states and were left at their default values.

2.3 The Lund $O(\alpha_s^2)$ model

JETSET 6.3 contains in addition a second order matrix element (ME) parton generator implementing the calculations of [21]. There is already evidence [22–24] that these calculations, allowing at most 4-parton states, fail to reproduce the rates of 4-jet-like events observed at PETRA. Because of the complexity of calculating 3rd, let alone higher, order QCD contributions to jet cross sections in perturbation theory, which has not yet been achieved*, the only alternative perturbative approach is provided by the LLA. For the foreseeable future, the 2nd order calculation is hence the best ‘exact’ matrix element calculation available. As in [8], we keep the parton pair resolution parameter y_{\min} [25] fixed (at 0.02) for all results presented here. For the $O(\alpha_s^2)$ matrix element the QCD scale parameter is $\Lambda_{\overline{MS}}$. Hadronisation is imposed after the parton production according to the Lund string model as briefly discussed in Sect. 2.2.

3 Definition of observables

We study both global event shape observables and single track inclusive distributions, using charged particles only. Event shapes may be characterised by us-

* The coefficient of $(\alpha_s/\pi)^3$ in the expansion of the ratio of hadronic to muon pair cross sections, R , has recently been calculated [33]

ing the sphericity tensor:

$$T_{\alpha\beta} = \frac{\sum_{j=1}^N p_{j\alpha} p_{j\beta}}{\sum_{j=1}^N |\mathbf{p}_j|^2}$$

where the sums are over the N particles in the event. The eigenvalues Q_1, Q_2, Q_3 are ordered such that $Q_3 > Q_2 > Q_1$ and satisfying $Q_1 + Q_2 + Q_3 = 1$. The event axis is taken to be the sphericity axis, the eigenvector corresponding to Q_3 , and the event plane is that defined by the eigenvectors corresponding to Q_3 and Q_2 . The variables aplanarity

$$A = 3/2 Q_1 \quad 0 \leq A \leq 1/2$$

and sphericity

$$S = 3/2(Q_1 + Q_2) \quad 0 \leq S \leq 1$$

are commonly used to characterise events. Extreme two-jet events have $S=0$, whilst $S \rightarrow 1$ for spherical events. Extreme planar events have $A=0$. Closely related event observables are:

$$\langle p_{T_{in}}^2 \rangle = \langle p^2 \rangle Q_2 \quad \text{and} \quad \langle p_{T_{out}}^2 \rangle = \langle p^2 \rangle Q_1$$

where $p_{T_{in}}$ and $p_{T_{out}}$ are the particle momentum components transverse to the sphericity axis in and out of the event plane respectively. The particle momenta enter quadratically into the sphericity tensor, so that the sphericity axis is more sensitive to high momentum tracks than, for example, the thrust axis, where the thrust T is defined:

$$T = \frac{\text{Max} \sum_{j=1}^N |p_{\parallel j}|}{\sum_{j=1}^N |\mathbf{p}_j|} \quad 1/2 \leq T \leq 1$$

the axis being chosen to maximise $\sum |p_{\parallel j}|$. Extreme two-jet events have $T=1$. Particle rapidity is defined

$$y = \frac{1}{2} \ln \left(\frac{E + p_{\parallel}}{E - p_{\parallel}} \right)$$

with respect to the thrust axis. A commonly used fragmentation variable is the scaled track momentum $x_p = 2|\mathbf{p}|/\sqrt{s}$.

The scaled invariant mass-squared of the two hemispheres in the event, $M_h^2/s, M_l^2/s$, are well-behaved quantities in perturbative calculations. Here the event is divided into two hemispheres by the plane perpendicular to the sphericity axis and 'h' denotes

the hemisphere with the greater mass, 'l' that with the lower mass. Because we use only charged particles in this analysis we divide the mass-squared by the *visible* energy-squared, E_{vis}^2 , rather than by s , where the pion mass is assumed for all particles measured in the tracking chambers.

4 Particle and event selection

The data were taken with the TASSO detector at PETRA at a centre of mass energy $W=35$ GeV. Details of the detector may be found in [26]. The selection of multihadronic final states from e^+e^- annihilation was based upon the information on charged particle momenta measured in the central detector. The selection criteria for charged particles and for multihadron events are described in detail in [1], but the main requirements are: a charged track must have a momentum component transverse to the beam $p_{xy} > 0.1$ GeV and a cosine of the polar angle $|\cos \theta| < 0.87$. The r.m.s. momentum resolution including multiple scattering is $\sigma_p/p = 0.016(1 + p^2)^{1/2}$, with p in GeV. The main criterion for multihadron events is based on the momentum sum of the accepted charged particles, $\sum_j p_j > 0.265 W$. In the 1986 running period

31 176 such events were measured.

To ensure a large acceptance for the particles in jets, only events with $|\cos \theta_{jet}| < 0.7$ were considered, where θ_{jet} is the angle between the sphericity axis and the beam axis. Events with a hard photon in the initial state were suppressed by requiring $|\cos \theta_n| > 0.2$, where θ_n is the angle between the normal to the event plane and the beam direction. From the initial sample of 31 176 events, 18 849 survived these cuts and were used in the subsequent analysis.

5 Backgrounds to the data sample

The backgrounds to the single photon (or Z^0) hadronic data sample from $\gamma\gamma$ scattering and τ pair production events were estimated by Monte Carlo simulation and found to be $0.91 \pm 0.10\%$, $0.72 \pm 0.03\%$ respectively *before* the cuts in θ_{jet}, θ_n , in agreement with previous estimates [1, 7], and $0.35 \pm 0.05\%$, $0.35 \pm 0.02\%$ *after* the event topology cuts. The background from beam gas interactions was negligible at this energy [1]. Whilst the percentage contamination to the data sample is small, certain ranges of some observables are especially sensitive to background and are expected to be heavily contaminated. For example, the first few bins of the charged multiplicity distribution are estimated to contain a large proportion of $\gamma\gamma$ and τ events which are typically of low multiplicity, whilst the latter, having in general a few

very energetic tracks, also populate bins of high x_p . To take this into account, the properly normalised background was subtracted from each distribution on a bin-by-bin basis.

6 Parameter tuning

No attempt was made to optimise each model simultaneously to the large number of different observables described in Sect. 3. It is clear that for any fit of a model to data, the larger the number of distributions fitted the worse will be the overall fit, unless there are strong correlations between the various observables, in which case it would be foolish to fit them all at once. Instead, a small set of relatively uncorrelated distributions of both event and single track observables, which are especially sensitive to the parameters to be fitted, was chosen, namely:

(1) Sphericity, S

(2) Particle momentum transverse to the event plane, $p_{T_{\text{out}}}$

(3) Particle momentum fraction, x_p

(4) Particle multiplicity per event n_{ch}

where only charged particles were used. This set contains two event and two track variables. S is dominated by properties in the event plane ($Q_2 \gg Q_1$) and is hence roughly orthogonal to $p_{T_{\text{out}}}$. The former is sensitive to hard gluon radiation in the event plane whilst the latter is sensitive to softer gluons and p_T arising from the hadronisation process. x_p is sensitive to the longitudinal fragmentation of jets, as is the event multiplicity n_{ch} . These distributions are hence suitable for determining optimum values of the parameters for both the perturbative QCD processes (A, Q_0) and the hadronisation (M_c, a, b, σ).

We use a method similar to that of a previous publication [2]. For each model, n_g values of each of the n_p parameters were used to define a grid in a parameter space of dimension n_p . For each of the $n_g^{n_p}$ points in the grid, Monte Carlo events were generated with QED radiative corrections and put through the detector simulation program and hadronic event selection procedures, giving roughly 5000 events remaining. Distributions of the observables, normalised per event, were produced for each MC dataset and also for the background-subtracted TASSO data. For

each bin of each distribution to be fitted, for every MC dataset the χ^2 was calculated between the MC and the same bin for the data. A second order polynomial in the n_p tuning parameters was then fitted to the $n_g^{n_p}$ χ^2 's for that bin. The sum of the polynomials, over all bins in all distributions was then minimised using the program MINUIT [27] to obtain the tuned values of the parameters.

An important point to note is that by this procedure the models (after detector simulation etc.) were compared with the essentially 'raw' TASSO data (after background subtraction). An alternative approach would have been to tune the models directly to the fully-corrected data, where the correction factors (see Sect. 7) were themselves determined from MC studies using the models. The former procedure is clearly less prone to possible biasing of the model tuning results than the latter.

The tuned parameters are shown in Table 1, together with the default values and the values obtained by Mark II [8] for comparison. Any one parameter may be varied by $\sim \pm 10\%$ from the optimum value with minimal effect on the description of the data. However, for the Lund cascade model (Table 1b) we found that a, b could be varied simultaneously across a wide range so as to preserve the agreement of the n_{ch} distribution with the data, and were only strongly constrained by the fit to x_p (see Sect. 8). This degree of freedom in a, b was much less evident for the Lund $O(\alpha_s^2)$ model (Table 1c), a reflection of the greater influence of the string fragmentation on the hadronic final state for the matrix element generator as compared to the cascade. The tuned values, of a, b shown in Tables 1b and c give a satisfactory description of the momentum spectrum of primary $D^{*\pm}$ mesons measured in high energy e^+e^- annihilation experiments [28].

Probably because of the $a-b$ correlation, the Mark II optimum values for the Lund models are somewhat different than ours, and they also obtain a good description of their data at 29 GeV. This allows a thorough and rigorous testing of the QCD models, in that they can only be fairly judged and compared after exploration of the range of their predictions arising from reasonable variations of their arbitrary parameters.

Table 1a. Parameters for the Webber cascade model

Parameter	Default	Tuning range	Tuned value	Mark II
QCD LLA scale A_{LL} (GeV)	0.35	0.1–0.5	0.25	0.20
Cascade virtuality cutoff Q_0 (GeV)	0.75	0.6–2.0	0.61	0.75
Cluster-mass parameter M_c (GeV/c ²)	3.75	2.0–4.0	2.3	3.0

Table 1 b. Parameters for the Lund cascade model

Parameter	Default	Tuning range	Tuned value	Mark II
QCD LLA scale A_{LL} (GeV)	0.40	0.15–1.2	0.26	0.40
Cascade virtuality cutoff Q_0 (GeV) ^a	1.0	0.5 –2.0	1.0	1.0
Fragmentation function parameter α	0.50	0.1 –1.0	0.18	0.45
Fragmentation function parameter b	0.90	0.1 –1.0	0.34	0.90
Gaussian p_T parameter $\sqrt{2\sigma}$ (GeV/c)	0.35	0.33–0.42	0.39	0.33

^a This parameter was not tuned simultaneously with the others, but was varied in the range shown after the optimum values of A_{LL} , a , b , σ had been found

Table 1 c. Parameters for the Lund $O(\alpha_s^2)$ model

Parameter	Default	Tuning range	Tuned value	Mark II
QCD scale in $O(\alpha_s^2)$ A_{MS} (GeV)	0.50	0.2–1.1	0.62	0.50
Parton pair resolution parameter y_{min}	0.02	Fixed ^a	0.02	0.015
Fragmentation function parameter a	1.0	0.1–1.0	0.58	0.9
Fragmentation function parameter b	0.7	0.2–1.1	0.41	0.7
Gaussian p_T parameter $\sqrt{2\sigma}$ (GeV/c)	0.40	Fixed ^a	0.40	0.33

^a In previous analyses [7] this parameter was found to be well-constrained by the data

7 Corrections to the data

The distributions presented below were corrected for acceptance, detector effects, initial state radiation and the cuts described in Sect. 4 using a Monte Carlo simulation [15] with our tuned parameters of Table 1 b. Initially, N_{gen} events were generated at $W=35$ GeV, with no QED radiative corrections, yielding the distributions $n_{gen}(x)$ of charged particles produced either in the fragmentation process or coming from the decay of particles with lifetimes less than $3 \cdot 10^{-10}$ s. A second set of events was then generated, including QED radiative effects, and traced through a simulation of the TASSO detector, thereby producing hits in the tracking chambers. Energy loss, multiple scattering, photon conversion and nuclear interactions in the material of the detector as well as decays were taken into account. The events were then passed through the track reconstruction and acceptance programs used for the real data, yielding N_{det} accepted events corresponding to the distributions of observables $n_{det}(x)$.

A correction factor $C^i(x)$ for every bin i of every distribution x was then defined:

$$C^i(x) = \frac{n_{gen}^i(x)}{N_{gen}} \bigg/ \frac{n_{det}^i(x)}{N_{det}}$$

The corrected distribution $n_{corr}^i(x)$ is then derived from the measured distribution $n_{meas}^i(x)$:

$$n_{corr}^i(x) = C^i(x) n_{meas}^i(x).$$

These correction factors $C^i(x)$ lie mainly in the range $0.7 < C^i(x) < 1.4$, though they are typically rather close to unity.

To estimate the systematic error in the correction process, this procedure was repeated using an independent jet fragmentation event generator [2, 29], yielding a second set of correction factors. The systematic error was taken to be the difference between the two sets of correction factors, though this was generally rather small.

The ‘true’ sphericity and thrust axes as well as the correction factors for the S , T and A distributions were determined using all (charged and neutral) particles which were either prompt or produced by the decay of particles with lifetimes less than $3 \cdot 10^{-10}$ s. The correction factors for all other quantities were calculated for charged particles only.

Using a Lund Monte Carlo simulation, the charged multiplicity distribution was unfolded as described in [1]. $n_{ch}=2, 4$ were taken from the Monte Carlo calculations. The systematic uncertainty in the unfolding procedure was estimated by using a Webber Monte Carlo simulation, the error being taken as the difference between the Lund and Webber unfolded values.

8 Comparison of the data with the models at $W=35$ GeV

For each model, the tuned parameter sets given above were used to generate 50000 MC events at

Table 2. Sphericity. The errors include the statistical error and that from the correction procedure

Sphericity range	$1/N_{ev} dN/dS$
0.00–0.02	3.47 ± 0.47
0.02–0.04	9.88 ± 0.28
0.04–0.06	8.39 ± 0.40
0.06–0.08	6.19 ± 0.46
0.08–0.10	4.40 ± 0.36
0.10–0.12	3.09 ± 0.17
0.12–0.14	2.47 ± 0.12
0.14–0.16	1.87 ± 0.11
0.16–0.18	1.43 ± 0.13
0.18–0.20	1.17 ± 0.09
0.20–0.22	0.89 ± 0.10
0.22–0.24	0.85 ± 0.09
0.24–0.28	0.66 ± 0.07
0.28–0.32	0.53 ± 0.04
0.32–0.40	0.34 ± 0.04
0.40–0.48	0.21 ± 0.03
0.48–0.60	0.12 ± 0.01
0.60–1.00	0.022 ± 0.003
Mean	0.113 ± 0.006

$W=35$ GeV, with no QED radiative corrections, no decays of particles with lifetimes greater than 3×10^{-10} s and no simulation of the detector. Distributions of the observables were then produced for each of these MC datasets and are shown in Figs. 1–14 compared to the fully-corrected 1986 TASSO data at $W=35$ GeV, also given in Tables 2–12. The lines shown in the figures connect the Monte Carlo calculated points. Unless otherwise stated, the errors on the data are the sum in quadrature of the statistical errors, the uncertainty in the background subtraction and the errors from the correction procedure described in Sect. 7. For most distributions any additional systematic errors are estimated [1] to be of similar magnitude to the given errors. For the x_p distribution the total systematic errors are estimated to be 5% for $x_p < 0.05$; 4% for $0.05 < x_p < 0.7$ and 10% for $x_p > 0.7$ [1, 7].

The Webber model gives too many spherical events (Fig. 1), and too many events of high aplanarity (Fig. 2). The thrust (Fig. 3) is poorly described; the distribution is smeared about the peak at $T \sim 0.94$ giving both an excess of events at high T and also in the low- T tail. There are too many high $\langle p_{T_{in}}^2 \rangle$ events (Fig. 4) whilst the high tail of $\langle p_{T_{out}}^2 \rangle$ is well-represented (Fig. 5), though there is an excess in the first few bins at low p_T . The charged particle multiplicity distribution is shown in Fig. 6; the model produces too many high multiplicity events, the mean being $\langle n_{ch} \rangle = 14.2$ compared to 13.6 ± 0.5 (total error) in the data. Turning to single particle distributions,

Table 3. Aplanarity. The errors include the statistical error and that from the correction procedure

Aplanarity range	$1/N_{ev} dN/dA$
0.00–0.01	22.5 ± 1.5
0.01–0.02	30.0 ± 0.7
0.02–0.03	17.8 ± 0.8
0.03–0.04	11.3 ± 0.5
0.04–0.05	6.35 ± 0.30
0.05–0.06	4.00 ± 0.23
0.06–0.07	2.24 ± 0.22
0.07–0.08	1.65 ± 0.14
0.08–0.09	1.04 ± 0.11
0.09–0.10	0.73 ± 0.08
0.10–0.30	0.108 ± 0.008
Mean	0.0237 ± 0.0007

Table 4. Thrust. The errors include the statistical error and that from the correction procedure

Thrust range	$1/N_{ev} dN/dT$
0.50–0.60	0.001 ± 0.001
0.60–0.64	0.05 ± 0.02
0.64–0.68	0.19 ± 0.03
0.68–0.72	0.30 ± 0.04
0.72–0.76	0.55 ± 0.04
0.76–0.80	0.79 ± 0.09
0.80–0.84	1.45 ± 0.12
0.84–0.88	2.53 ± 0.22
0.88–0.90	4.38 ± 0.17
0.90–0.92	7.02 ± 0.38
0.92–0.94	9.63 ± 0.44
0.94–0.96	10.44 ± 0.40
0.96–0.98	5.80 ± 0.33
0.98–1.00	0.82 ± 0.21
Mea	0.906 ± 0.018

Table 5. $\langle p_{T_{in}}^2 \rangle$. The errors include the statistical error and that from the correction procedure

$\langle p_{T_{in}}^2 \rangle$ range	$1/N_{ev} dN/d\langle p_{T_{in}}^2 \rangle$
0.00–0.05	0.99 ± 0.07
0.05–0.10	4.35 ± 0.11
0.10–0.15	4.23 ± 0.10
0.15–0.20	2.89 ± 0.10
0.20–0.25	1.93 ± 0.08
0.25–0.30	1.18 ± 0.05
0.30–0.35	0.96 ± 0.07
0.35–0.40	0.72 ± 0.06
0.40–0.45	0.52 ± 0.04
0.45–0.50	0.38 ± 0.03
0.50–0.60	0.27 ± 0.02
0.60–0.75	0.16 ± 0.01
0.75–1.00	0.083 ± 0.007
1.00–2.50	0.011 ± 0.003
Mean	0.238 ± 0.009

Table 6. $\langle p_{T_{out}}^2 \rangle$. The errors include the statistical error and that from the correction procedure

$\langle p_{T_{out}}^2 \rangle$ range	$1/N_{ev} dN/d\langle p_{T_{out}}^2 \rangle$
0.00–0.01	0.47 ± 0.10
0.01–0.02	3.66 ± 0.22
0.02–0.03	9.33 ± 0.31
0.03–0.04	12.50 ± 0.43
0.04–0.05	13.60 ± 0.41
0.05–0.06	13.40 ± 0.62
0.06–0.07	10.61 ± 0.55
0.07–0.08	8.49 ± 0.36
0.08–0.09	6.68 ± 0.32
0.09–0.10	5.00 ± 0.28
0.10–0.11	3.98 ± 0.31
0.11–0.12	2.50 ± 0.24
0.12–0.13	1.98 ± 0.17
0.13–0.15	1.56 ± 0.11
0.15–0.20	0.71 ± 0.05
0.20–0.50	0.064 ± 0.008
Mean	0.071 ± 0.001

Table 7. The n_{ch} distribution unfolded using a Lund Monte Carlo simulation. The first error is statistical and the second is the systematic uncertainty (see text)

n_{ch}	$1/N_{ev} dN/dn_{ch} (\times 10^{-3})$
2	0.4 ± 0.5 ± 0.0
4	5.9 ± 0.8 ± 0.6
6	32.3 ± 1.5 ± 0.2
8	84.4 ± 2.2 ± 1.7
10	153.4 ± 3.0 ± 4.3
12	197.4 ± 3.4 ± 8.2
14	191.6 ± 3.4 ± 7.3
16	143.8 ± 2.9 ± 4.3
18	91.7 ± 2.3 ± 6.7
20	50.7 ± 1.7 ± 8.5
22	27.3 ± 1.2 ± 1.4
24	12.4 ± 0.8 ± 0.8
26	5.2 ± 0.5 ± 0.5
28	2.0 ± 0.3 ± 0.5
30	0.8 ± 0.2 ± 0.1
32	0.4 ± 0.2 ± 0.3
34	0.1 ± 0.1 ± 0.1
Mean	13.58 ± 0.02 ± 0.46

$p_{T_{in}}$, $p_{T_{out}}$, p_T and x_p (Figs. 7, 8, 9, 10 respectively) are well described, though there is a slight excess of $p_{T_{in}}$ in the tail. Rapidity (Fig. 11) is not so well described, the MC giving too many particles for $y > 3$. M_h^2/s , M_l^2/s (Figs. 12, 13) are poorly represented with a large excess of events of low mass, though the description of $(M_h^2 - M_l^2)/s$ (Fig. 14) is much better.

The general conclusion is that quantities related to p_T out of the event plane are reasonably well-described, whilst those related to p_T in the plane are

Table 8. $p_{T_{in}}$. The errors include the statistical error and that from the correction procedure

$p_{T_{in}}$ range	$1/N_{ev} dN/dp_{T_{in}}$
0.0–0.1	37.32 ± 0.68
0.1–0.2	29.40 ± 0.49
0.2–0.3	21.41 ± 0.42
0.3–0.4	14.84 ± 0.26
0.4–0.5	10.55 ± 0.19
0.5–0.6	7.40 ± 0.10
0.6–0.7	5.29 ± 0.17
0.7–0.8	3.86 ± 0.08
0.8–0.9	2.83 ± 0.06
0.9–1.0	2.14 ± 0.09
1.0–1.1	1.47 ± 0.04
1.1–1.2	1.17 ± 0.06
1.2–1.3	0.91 ± 0.03
1.3–1.4	0.67 ± 0.03
1.4–1.5	0.62 ± 0.04
1.5–1.6	0.41 ± 0.03
1.6–1.8	0.32 ± 0.01
1.8–2.0	0.22 ± 0.01
2.0–2.5	0.103 ± 0.006
2.5–3.0	0.036 ± 0.006
3.0–5.0	0.008 ± 0.001
Mean	0.331 ± 0.002

Table 9. $p_{T_{out}}$. The errors include the statistical error and that from the correction procedure

$p_{T_{out}}$ range	$1/N_{ev} dN/dp_{T_{out}}$
0.00–0.05	53.0 ± 1.0
0.05–0.10	46.34 ± 0.84
0.10–0.15	40.44 ± 0.74
0.15–0.20	33.82 ± 0.50
0.20–0.25	26.90 ± 0.49
0.25–0.30	21.64 ± 0.36
0.30–0.35	16.46 ± 0.43
0.35–0.40	12.14 ± 0.21
0.40–0.45	9.18 ± 0.24
0.45–0.50	6.72 ± 0.15
0.50–0.55	4.84 ± 0.12
0.55–0.60	3.56 ± 0.11
0.60–0.65	2.60 ± 0.11
0.65–0.70	2.06 ± 0.12
0.70–0.80	1.15 ± 0.04
0.80–0.90	0.64 ± 0.03
0.90–1.00	0.33 ± 0.03
1.00–2.00	0.050 ± 0.003
Mean	0.201 ± 0.001

overestimated at high p_T . The latter is probably partly influenced by the low value of the mass above which clusters are split into two, $M_c = 2.3$ GeV/c², determined from the tuning. Our results are in general agreement with those of Mark II [8], with minor differences in some distributions. The total χ^2 is 942

Table 10. p_T . The errors include the statistical error and that from the correction procedure

p_T range	$1/N_{ev} dN/dp_T$
0.0–0.1	12.68 \pm 0.19
0.1–0.2	25.16 \pm 0.49
0.2–0.3	26.25 \pm 0.64
0.3–0.4	21.43 \pm 0.36
0.4–0.5	15.85 \pm 0.20
0.5–0.6	11.37 \pm 0.14
0.6–0.7	7.96 \pm 0.20
0.7–0.8	5.68 \pm 0.12
0.8–0.9	4.08 \pm 0.09
0.9–1.0	2.91 \pm 0.11
1.0–1.1	1.98 \pm 0.05
1.1–1.2	1.52 \pm 0.05
1.2–1.3	1.16 \pm 0.04
1.3–1.4	0.85 \pm 0.04
1.4–1.5	0.74 \pm 0.06
1.5–1.6	0.51 \pm 0.03
1.6–1.8	0.36 \pm 0.02
1.8–2.0	0.23 \pm 0.01
2.0–2.5	0.117 \pm 0.006
2.5–3.0	0.038 \pm 0.006
3.0–5.0	0.008 \pm 0.001
Mean	0.425 \pm 0.003

Table 11. x_p . The errors include the statistical error and that from the correction procedure

x_p range	$1/N_{ev} dN/dx_p$
0.00–0.02	121.0 \pm 1.5
0.02–0.04	161.9 \pm 2.5
0.04–0.06	107.6 \pm 2.1
0.06–0.08	72.0 \pm 1.8
0.08–0.10	51.5 \pm 1.1
0.10–0.12	37.06 \pm 0.88
0.12–0.14	29.95 \pm 1.17
0.14–0.16	22.88 \pm 0.55
0.16–0.18	17.97 \pm 0.35
0.18–0.20	14.50 \pm 0.36
0.20–0.22	12.67 \pm 0.50
0.22–0.24	9.66 \pm 0.35
0.24–0.26	8.22 \pm 0.35
0.26–0.28	6.99 \pm 0.38
0.28–0.30	5.68 \pm 0.21
0.30–0.32	4.76 \pm 0.20
0.32–0.34	3.90 \pm 0.17
0.34–0.36	3.49 \pm 0.21
0.36–0.38	2.73 \pm 0.15
0.38–0.40	2.59 \pm 0.15
0.40–0.44	1.95 \pm 0.09
0.44–0.48	1.52 \pm 0.08
0.48–0.52	1.02 \pm 0.07
0.52–0.60	0.71 \pm 0.04
0.60–0.70	0.32 \pm 0.03
0.70–1.00	0.07 \pm 0.02
Mean	0.0877 \pm 0.0007

Table 12. Rapidity. The errors include the statistical error and that from the correction procedure

Rapidity range	$1/N_{ev} dN/dy$
0.0–0.2	459 \pm 0.09
0.2–0.4	5.03 \pm 0.06
0.4–0.6	5.09 \pm 0.08
0.6–0.8	5.15 \pm 0.07
0.8–1.0	5.40 \pm 0.12
1.0–1.2	5.43 \pm 0.14
1.2–1.4	5.41 \pm 0.14
1.4–1.6	5.27 \pm 0.14
1.6–1.8	5.12 \pm 0.17
1.8–2.0	4.88 \pm 0.19
2.0–2.2	4.55 \pm 0.20
2.2–2.4	3.86 \pm 0.11
2.4–2.6	3.25 \pm 0.10
2.6–2.8	2.61 \pm 0.06
2.8–3.0	1.85 \pm 0.04
3.0–3.2	1.36 \pm 0.03
3.2–3.4	0.90 \pm 0.03
3.4–3.6	0.56 \pm 0.03
3.6–3.8	0.35 \pm 0.02
3.8–4.0	0.20 \pm 0.01
4.0–4.2	0.12 \pm 0.01
4.2–4.4	0.066 \pm 0.007
4.4–4.6	0.035 \pm 0.004
4.6–4.8	0.013 \pm 0.003
4.8–5.0	0.006 \pm 0.002
Mean	1.45 \pm 0.01

for 245 data points, though correlations between many of the observables make this number difficult to interpret.

The Lund $O(\alpha_s^2)$ model reproduces the sphericity distribution very accurately (Fig. 1), though gives far too few events of high aplanarity (Fig. 2). Thrust is much better described than by the Webber model (Fig. 3), though the peak is shifted to slightly lower T values than the data. There are slightly too many high $\langle p_{T_{in}}^2 \rangle$ events (Fig. 4) and too few high $\langle p_{T_{out}}^2 \rangle$ events (Fig. 5). $p_{T_{in}}$ and p_T are very well described (Figs. 7, 9) though there is a deficiency of high $p_{T_{out}}$ tracks (Fig. 8). The charged multiplicity distribution (Fig. 6), x_p (Fig. 10) and rapidity (Fig. 11) are well described, though there are too few tracks in the range $1.4 < y < 2.4$; $\langle n_{ch} \rangle = 13.8$. The M^2/s distributions (Figs. 12–14) are reproduced satisfactorily.

Overall, the $p_{T_{in}}$ -related quantities are accurately reproduced, whilst $p_{T_{out}}$ quantities are seriously underestimated for high p_T ; there are slightly too few high thrust events. These results are in good agreement with Mark II. The quality of description of the data by the MC is much better than for the Webber model, with a total χ^2 of 658.

The best description of the data is provided by the Lund cascade model, which gives a generally good

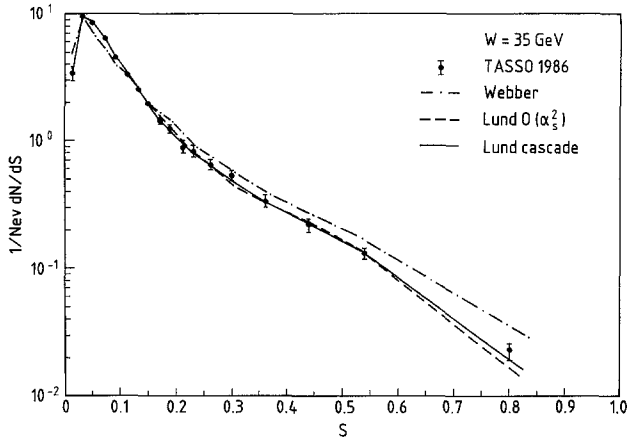


Fig. 1. The sphericity distribution at $W=35$ GeV

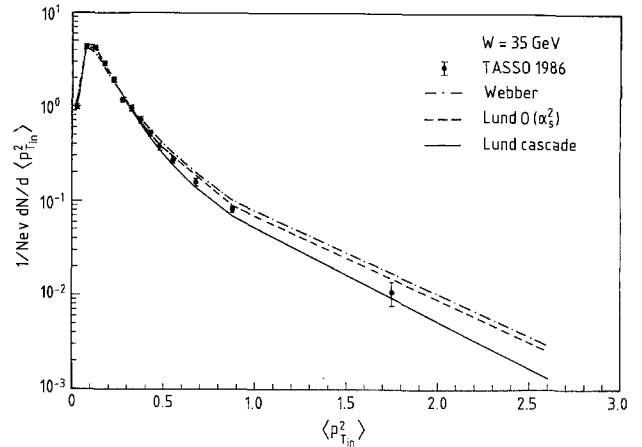


Fig. 4. The $\langle p_{T,in}^2 \rangle$ distribution at $W=35$ GeV

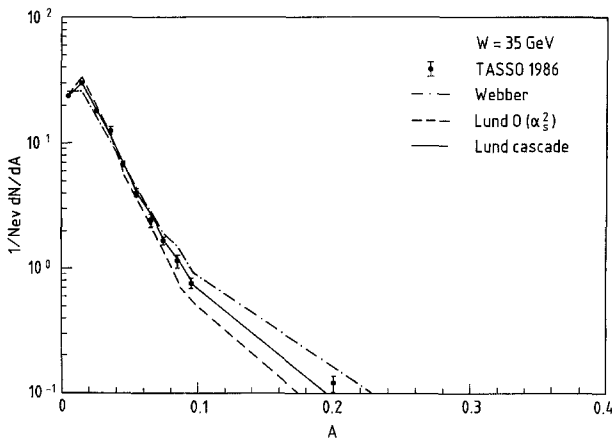


Fig. 2. The aplanarity distribution at $W=35$ GeV

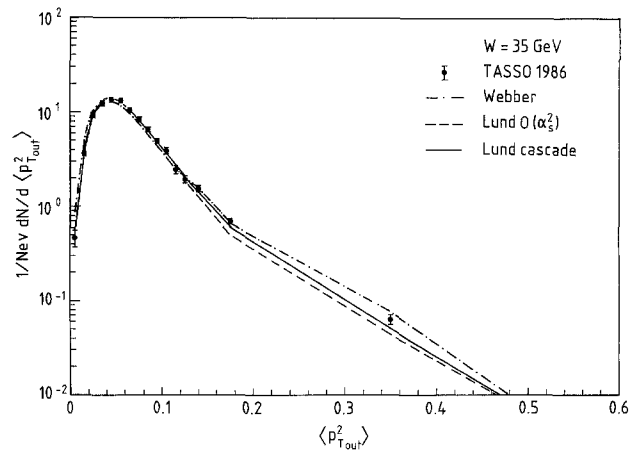


Fig. 5. The $\langle p_{T,out}^2 \rangle$ distribution at $W=35$ GeV

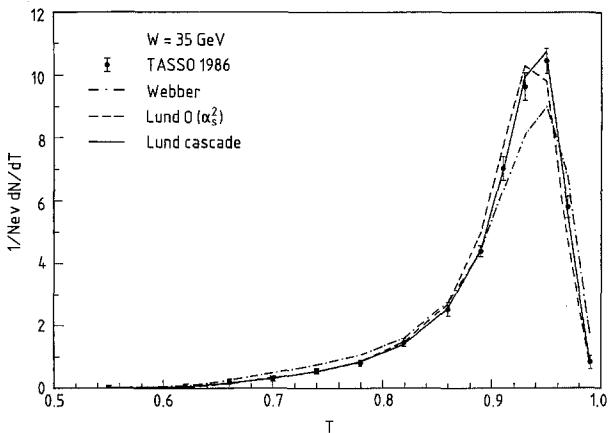


Fig. 3. The thrust distribution at $W=35$ GeV

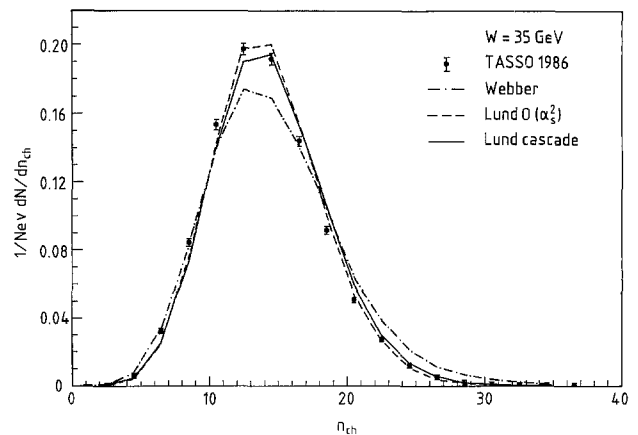


Fig. 6. The charged particle multiplicity distribution at $W=35$ GeV. The data were unfolded using a Lund Monte Carlo simulation; the errors are statistical only

description of all observables, though inevitably with some discrepancies in some bins of certain distributions. The most serious examples are the underestimations of the high $p_{T,in}$ and p_T tails (Figs. 7, 9). Of particular note is the excellent description of the thrust

distribution (Fig. 3), which many models have had difficulty with in the past. In these observations we agree with the Mark II results, with only one major exception: we do not observe the serious shortfall of tracks at $x_p > 0.7$ seen in [8]. This is because of the

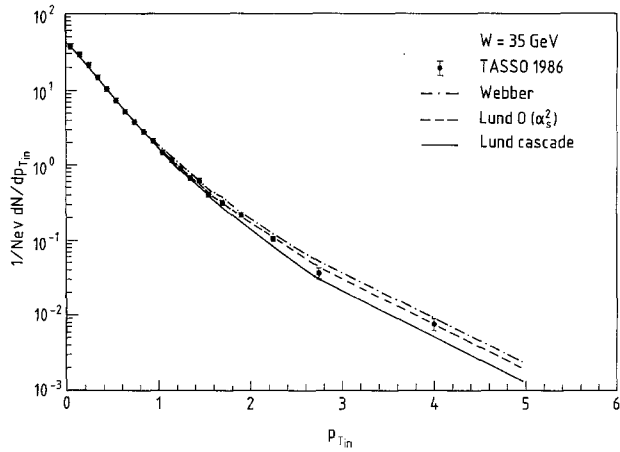


Fig. 7. The $p_{T,in}$ distribution at $W=35$ GeV

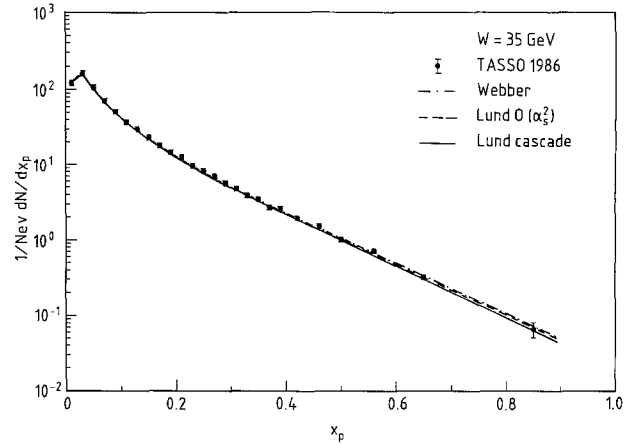


Fig. 10. The x_p distribution at $W=35$ GeV

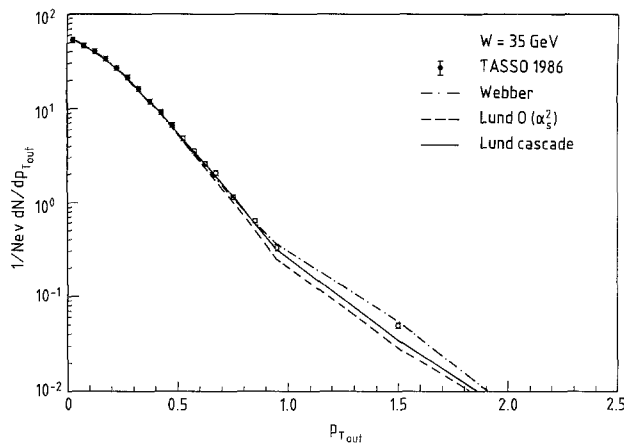


Fig. 8. The $p_{T,out}$ distribution at $W=35$ GeV

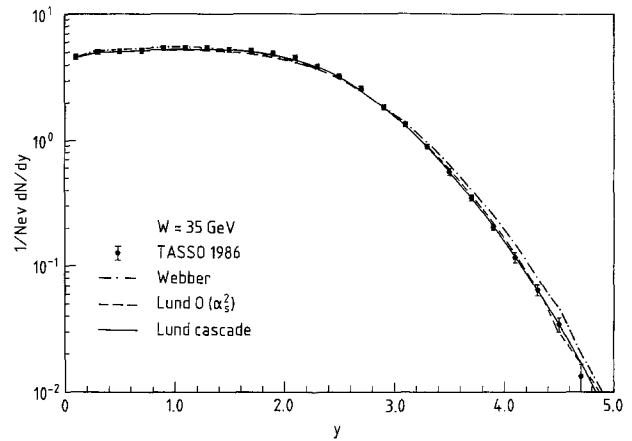


Fig. 11. The rapidity distribution at $W=35$ GeV

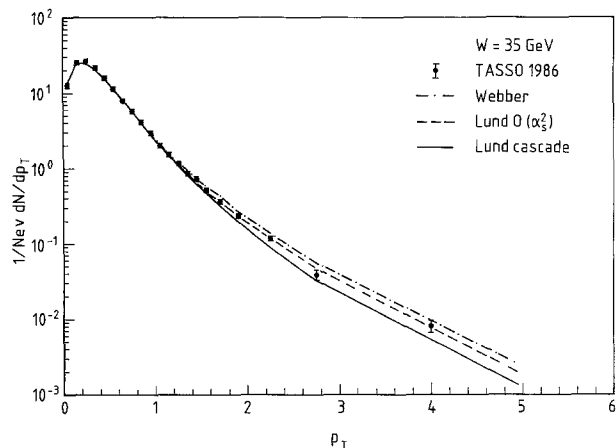


Fig. 9. The p_T (relative to the sphericity axis) distribution at $W=35$ GeV

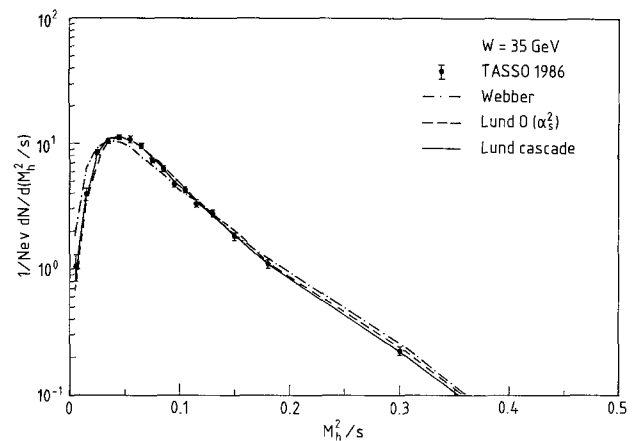


Fig. 12. The M_h^2/s distribution at $W=35$ GeV

different values of the fragmentation parameters (a , b) used in the comparisons. We have found that the combination (0.18, 0.34) actually gives a very similar x_p spectrum to the default combination (0.5, 0.9), except in the region $x_p > 0.6$, where the latter falls well

below the former. The Mark II tuned values, (0.45, 0.9) are clearly very close to the default and it is therefore no surprise that they find a much lower MC result in this region of x_p . The M^2/s distributions (Figs. 12–14) are well represented. The overall χ^2 is 367.

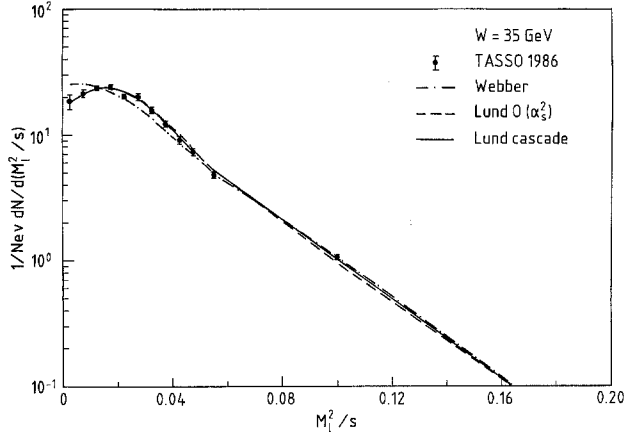


Fig. 13. The M_T^2/s distribution at $W=35$ GeV

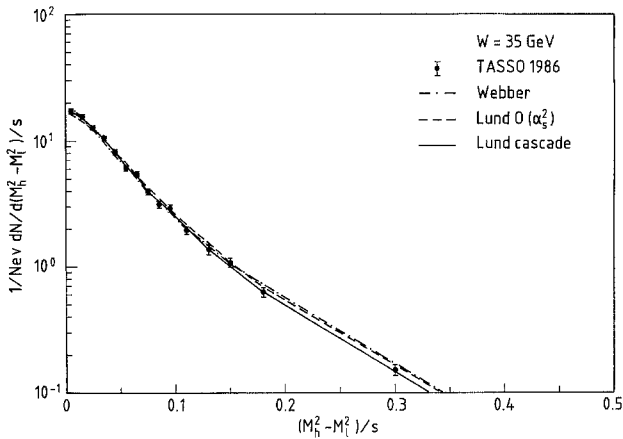


Fig. 14. The $(M_h^2 - M_T^2)/s$ distribution at $W=35$ GeV

The $O(\alpha_s^2)$ model seems to do well with the observables related to hard gluon radiation in the event plane, namely S , $\langle p_{T_{in}}^2 \rangle$, $p_{T_{in}}$, but does not give enough events of high A , $\langle p_{T_{out}}^2 \rangle$ or tracks of high $p_{T_{out}}$, even though the parameter σ , which basically controls these quantities, has a reasonable value. By contrast the LLA model (Webber cascade) is good for $p_{T_{out}}$ -like observables, but overestimates $p_{T_{in}}$ quantities. The LLA + $O(\alpha_s)$ ME model (Lund cascade) reproduces the $p_{T_{out}}$ -like distributions very well but gives too few events/tracks of high $p_{T_{in}}$, though it is generally better for these than the LLA model, which overestimates.

Given that Mark II finds the same effects using rather different values of the fragmentation parameters, we feel justified in concluding that it is likely that many of these effects arise chiefly from the QCD parts of the models rather than the hadronisation, though of course these two processes cannot be isolated completely in interpreting the model results. Indeed, it was found in [8] that the combination of

Webber LLA cascade + Lund string fragmentation gave somewhat better agreement with the data than the Webber cascade with cluster hadronisation. It is, however, perhaps not surprising that a better description of the data is provided by a model incorporating both LLA and $O(\alpha_s)$ ME QCD, thereby taking into account both hard and multiple soft gluon emission, rather than either LLA or $O(\alpha_s^2)$ QCD alone. (This $O(\alpha_s)$ ME feature could be implemented [31] in the new version of the Webber model [30].)

9 Energy evolution of the observables

A further test of the QCD fragmentation models is whether they are able, with the parameters optimised at one energy, to describe the evolution of the various observables across the range of energies explored at e^+e^- colliders to date. We present in Figs. 15–20 the mean values of some of the observables shown in Figs. 1–14, as a function of the c.m. energy W . In addition to the present measurements at $W=35$ GeV (labelled ‘this publication’), TASSO data are shown (labelled ‘TASSO 1984’) for the energy range $12.0 \leq \langle W \rangle \leq 41.5$ GeV from a previous publication [1], where the data were corrected using an independent jet Monte Carlo simulation including a QCD parton level calculation to $O(\alpha_s)$ [34]. Also shown are the MARK II [8] and HRS [4] results at $W=29$ GeV. Unless otherwise stated, the errors on the TASSO measurements from this analysis at $W=35$ GeV are the sum in quadrature of the statistical errors and the errors from the background subtraction and data correction; the errors on the previous TASSO data and the HRS data are statistical only; the Mark II errors are the sum in quadrature

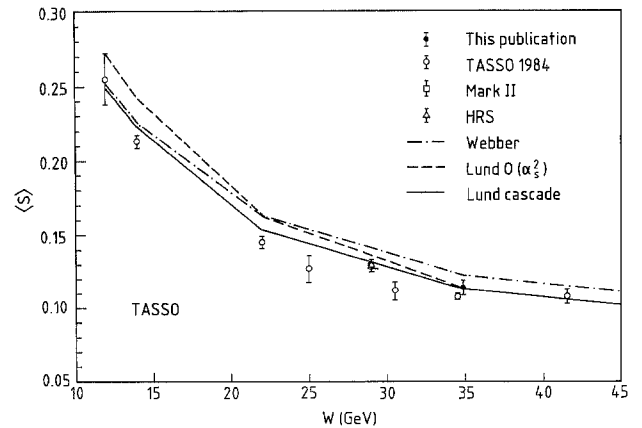


Fig. 15. The mean sphericity as a function of W for the TASSO data in the range $12 \leq W \leq 41.5$ GeV, the Mark II and HRS data at 29 GeV and for the models. The error shown on the 35 GeV data point includes the uncertainty arising from using two different Monte Carlo calculations to correct the data (Sect. 7)

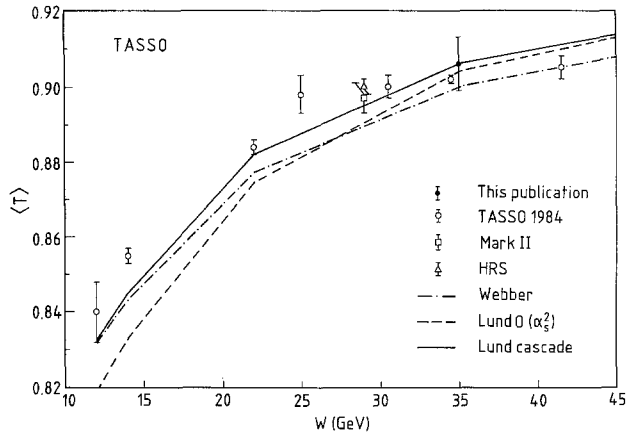


Fig. 16. The mean thrust as a function of W for the TASSO data in the range $12 \leq W \leq 41.5$ GeV, the Mark II and HRS data at 29 GeV and for the models. The error shown on the 35 GeV data point includes the uncertainty arising from using two different Monte Carlo calculations to correct the data (Sect. 7)

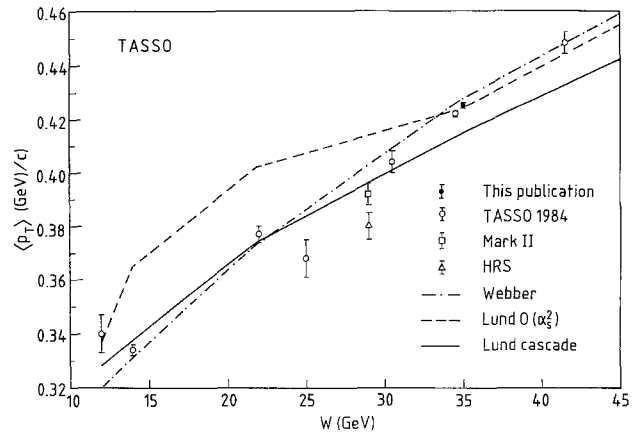


Fig. 18. The mean p_T as a function of W for the TASSO data in the range $12 \leq W \leq 41.5$ GeV, the Mark II and HRS data at 29 GeV and for the models. The error shown on the 35 GeV data point includes the uncertainty arising from using two different Monte Carlo calculations to correct the data (Sect. 7)

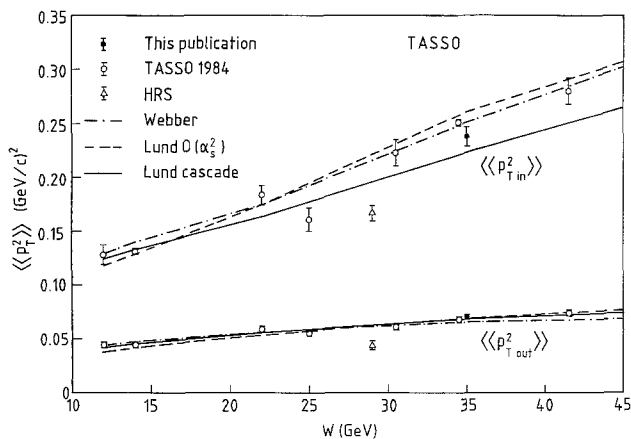


Fig. 17. The mean $\langle p_{T,in}^2 \rangle$ and $\langle p_{T,out}^2 \rangle$ as a function of W for the TASSO data in the range $12 \leq W \leq 41.5$ GeV, the HRS data at 29 GeV and for the models. The error shown on the 35 GeV data point includes the uncertainty arising from using two different Monte Carlo calculations to correct the data (Sect. 7)

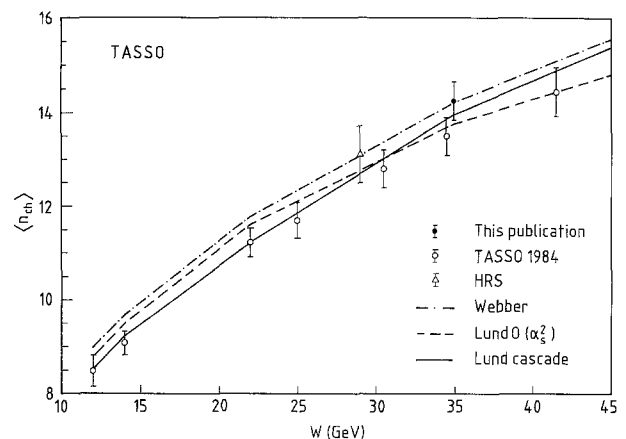


Fig. 19. The mean charged multiplicity as a function of W for the TASSO data in the range $12 \leq W \leq 41.5$ GeV, the HRS data at 29 GeV and for the models. The errors on the data include systematic effects (Sect. 7)

of the statistical errors and the uncertainty in the correction procedure.

The mean sphericity is shown in Fig. 15, where all the models reproduce the trend of the data, though all systematically overestimate $\langle S \rangle$ between 14 and 25 GeV. Interestingly, this effect was also seen by Mark II who tuned to their data at 29 GeV. Above 22 GeV the Webber cascade gives systematically higher sphericities than both the Lund models. The mean sphericity calculated for the data in the present analysis, where the correction factors were determined using an LLA + $O(\alpha_s)$ fragmentation model, is in agreement with that at $W = 34.5$ GeV from our previous publication, where the data were corrected using an $O(\alpha_s)$ fragmentation model.

$\langle T \rangle$ (Fig. 16) is reasonably described by all the models; the Lund cascade is probably the best. Webber is systematically lower than the data and the $O(\alpha_s^2)$ seriously underestimates below 34 GeV.

For $\langle p_{T,in}^2 \rangle^*$ (Fig. 17), both Webber and $O(\alpha_s^2)$ are better than the Lund cascade, which is systematically lower than most of the data. The HRS point at 29 GeV appears to be somewhat lower than the general trend of the TASSO data. The $\langle p_{T,out}^2 \rangle$ data (Fig. 17) are well described by all models, though again the HRS point (shown with systematic error included) lies below the TASSO data. $\langle p_{T,in}^2 \rangle$ in-

* The inner $\langle \rangle$ denotes averaging over all particles in an event and the outer $\langle \rangle$ denotes averaging over all events

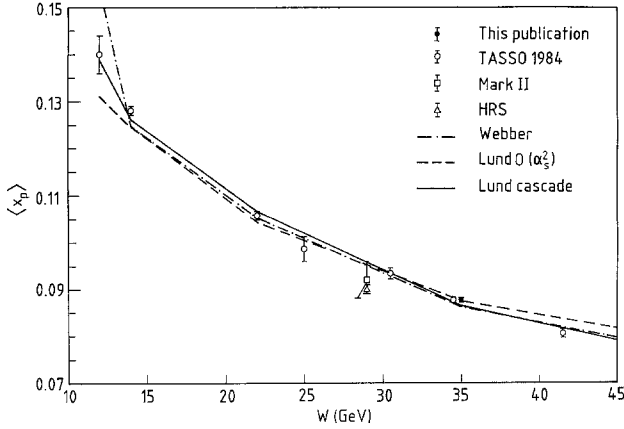


Fig. 20. The mean x_p as a function of W for the TASSO data in the range $12 \leq W \leq 41.5$ GeV, the Mark II and HRS data at 29 GeV and for the models. The error shown on the 35 GeV data point includes the uncertainty arising from using two different Monte Carlo calculations to correct the data (Sect. 7)

increases more rapidly with energy than $\langle p_{T_{out}}^2 \rangle$, reflecting the harder gluon emission in the event plane than out of it. The $\langle p_T \rangle$ evolution (Fig. 18) is well described by Webber; the Lund cascade is systematically low in the higher energy domain. The peculiar behaviour of the $O(\alpha_s^2)$ model is a consequence of the value of $A_{\overline{MS}} = 0.62$ GeV used; the default value $A_{\overline{MS}} = 0.50$ GeV used in conjunction with either the tuned values or the default values of a, b gives much better agreement with the data below 34 GeV.

Both the Lund models are in good agreement with the data for $\langle n_{ch} \rangle$; (Fig. 19). Webber is systematically around $\sim 0.5-1$ unit above the data, though in excellent agreement with the TASSO 1986 measurement. For $\langle x_p \rangle$ (Fig. 20), all models are in good agreement with the data, though the $O(\alpha_s^2)$ is somewhat soft below 22 GeV

10 Summary and conclusions

We have compared the three most successful perturbative QCD+fragmentation models with the high statistics data sample collected by TASSO at 35 GeV. Having optimised the important parameters of each model by comparison with the data for a few relevant observables, we find that all the models give a reasonable overall description of the global features of hadronic events at this energy, though the quality of description of different observables varies for each model.

The Lund model incorporating a LLA parton cascade interfaced with the $O(\alpha_s)$ ME provides a better overall representation of the data than either the Webber cascade or Lund $O(\alpha_s^2)$ models. We interpret the differences between the models as being due main-

ly to the different treatments of the parton level processes, with some inevitable lesser contribution from hadronisation effects. The $O(\alpha_s^2)$ ME described properties in the event plane, mainly determined by hard gluon bremsstrahlung, very well, but was deficient in the properties transverse to this plane, which are more sensitive to soft gluon and hadronisation effects. The LLA cascade gave a good description of the transverse observables, but overestimated those in the plane. The LLA cascade + $O(\alpha_s)$ ME provided a good representation of the transverse properties but underestimated some observables in the plane, though here the discrepancy between MC and data was much smaller than for the LLA cascade. This suggests that the amount of hard gluon radiation is somewhat underestimated, despite matching the $O(\alpha_s)$ ME onto the cascade to try and get this feature correct. It is tempting to suggest that the slight lack of gluon emission in the event plane could be made up by $O(\alpha_s^2)$ corrections to the $O(\alpha_s)$ ME, though this cannot of course be proved, and hadronisation effects are probably just as large as such corrections.

The evolution of the mean values of the observables as a function of c.m. energy over the range $12.0 \leq \sqrt{s} \leq 41.5$ GeV is generally well described by the models using the parameters optimised at 35 GeV.

Acknowledgements. We gratefully acknowledge the support of the DESY directorate, the PETRA machine group and the DESY computer centre. Those of us from outside DESY wish to thank the DESY directorate for the hospitality extended to us while working at DESY. We would like to thank M. Bengtsson, G. Ingelman, T. Sjöstrand and B. Webber for helpful discussions.

References

1. TASSO Coll. M. Althoff et al.: Z. Phys. C – Particles and Fields 22 (1984) 307
2. TASSO Coll. M. Althoff et al.: Z. Phys. C – Particles and Fields 26 (1984) 157
3. TASSO Coll. M. Althoff et al.: Z. Phys. C – Particles and Fields 29 (1985) 29; Mark II Coll. A. Petersen et al.: Phys. Rev. Lett. 55 (1985) 1954; TPC/Two-Gamma Coll. H. Aihara et al.: Z. Phys. C – Particles and Fields 28 (1985) 31
4. HRS Coll. D. Bender et al.: Phys. Rev. D 31 (1985) 1.
5. For a general review see D.H. Saxon: RAL-86-057 (1986)
6. JADE Coll. W. Bartel et al.: Phys. Lett. 101 B (1981) 129; JADE Coll. W. Bartel et al.: Z. Phys. C – Particles and Fields 21 (1983) 37; JADE Coll. W. Bartel et al.: Phys. Lett. 134 B (1984) 275; JADE Collab. W. Bartel et al.: Phys. Lett. 157 B (1985) 340
7. P. Dauncey: Oxford D. Phil. Thesis, RAL T 034 (1986)
8. Mark II Coll. A. Petersen et al.: Phys. Rev. D 37, (1988) 1
9. G. Marchesini, B.R. Webber: Nucl. Phys. B 238 (1984) 1; B.R. Webber: Nucl. Phys. B 238 (1984) 492
10. T. Sjöstrand, M. Bengtsson: Comput. Phys. Commun. 43 (1987) 367
11. T.D. Gottschalk: Nucl. Phys. B 214 (1983) 201; T.D. Gottschalk, D.A. Morris: Nucl. Phys. B 288 (1987) 729
12. T. Sjöstrand: Int. J. Mod. Phys. A 3 (1988) 751
13. G. Altarelli, G. Parisi: Nucl. Phys. B 126 (1977) 298

14. R. Odorico: *Z. Phys. C – Particles and Fields* C30 (1986) 257
15. M. Bengtsson, T. Sjöstrand: *Phys. Lett.* 185 B (1987) 435
16. G. Ingelman: *Phys. Scr.* 33 (1986) 39; P.N. Burrows, G. Ingelman: *Z. Phys. C – Particles and Fields* 34 (1987) 91
17. D. Amati et al.: *Nucl. Phys.* B173 (1980) 429; G. Curci, W. Furmanski, H. Petronzio: *Nucl. Phys.* B175 (1980) 27
18. B. Klima, DESY 86-070 (1986)
19. M. Bengtsson, T. Sjöstrand: *Nucl. Phys.* B289 (1987) 810
20. B. Andersson, G. Gustafson, G. Ingelman, T. Sjöstrand: *Phys. Rep.* 97 (1983) 33
21. F. Gutbrod, G. Kramer, G. Schierholz: *Z. Phys. C – Particles and Fields* 21 (1984) 235
22. JADE Coll. W. Bartel et al.: *Z. Phys. C – Particles and Fields* 33 (1986) 23
23. TASSO Coll. W. Braunschweig et al.: *Oxford Nuclear Physics* 29/88 and DESY 88-046 (1988)
24. S. Bethke: Heidelberg Habilitation Thesis, LBL 50-208 (1987)
25. G. Kramer, B. Lampe: DESY 86-119 (1986)
26. TASSO Coll. R. Brandelik et al.: *Phys. Lett.* 83 B (1979) 261; *Z. Phys. C – Particles and Fields* 4 (1980) 87
27. F. James, M. Roos: *Comput. Phys. Commun* 10 (1975) 343
28. TASSO Coll. M. Althoff et al.: *Phys. Lett.* 126 B (1983) 493; Mark II Coll. J.M. Yelton et al.: *Phys. Rev. Lett.* 49 (1982) 430; JADE Coll. W. Bartel et al.: *Phys. Lett.* 146 B (1984) 121; HRS Collab., M. Derrick et al.: *Phys. Lett.* 146 B (1984) 261
29. K. Fabricius et al.: *Phys. Lett.* 97 B (1980) 431, *Z. Phys. C – Particles and Fields* 11 (1982) 315
30. G. Marchesini, B.R. Webber: Cavendish-HEP-87/8 and 87/9 (1987)
31. B.R. Webber: private communications
32. P.N. Burrows: *Oxford Nuclear Physics* 43/88 (1988)
33. S.G. Gorishny et al.: *Proc. Conf. on Hadron Structure, Smolenice, Czechoslovakia, November 1987*, ed. D. Krupa, Vol. 14 *Physics and Applications*, Inst. of Phys. EPRC Slovak Academy of Sciences, Bratislava, 1988, and Dubna preprint JINR E2-88-254
34. P. Hoyer et al.: *Nucl. Phys.* B161 (1979) 34